MOUNTAIN-PLAINS CONSORTIUM

MPC 19-382 | H. Mahmoud and E. Hassan

Seismic Performance of Highway Embankments

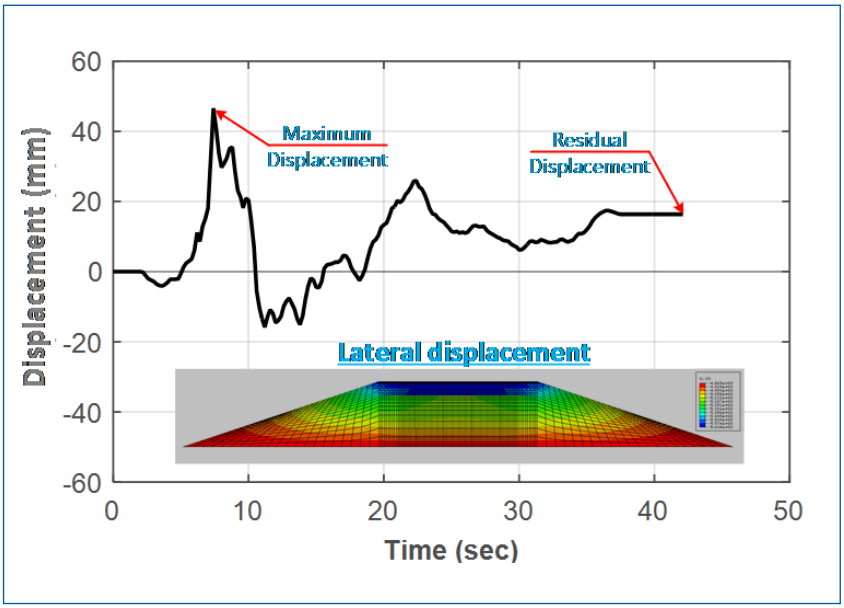

MOUNTAIN-PLAINS CONSORTIUM REGION 8

A University Transportation Center sponsored by the U.S. Department of Transportation serving the Mountain-Plains Region. Consortium members:

Colorado State University
North Dakota State University
South Dakota State University
University of Colorado Denver
University of Denver
University of Utah
Utah State University
University of Wyoming

Seismic Performance of Highway Embankments

Hussam Mahmoud
Emad M. Hassan

Department of Civil and Environmental Engineering
Colorado State University
Fort Collins, Colorado

April 2019

Acknowledgements

The funds for this study were provided, in part, by the United States Department of Transportation to the Mountain-Plains Consortium (MPC). Matching funds were provided by Colorado State University. The data for this study, provided by Colorado State Patrol and Colorado Department of Transportation, is greatly appreciated.

Disclaimer

TABLE OF CONTENTS

LIST OF FIGURES

LIST OF TABLES

1. INTRODUCTION

1.1 Background and Scope

Functional transportation networks are considered the backbone of modern societies. The reliance of various infrastructures, such as health, food, water, and commercial or transportation networks, cannot be overstated, particularly following natural disasters [1]. Vital needs, such as medical care, food, and water, are serviced by a functioning network of roads. One of the main hazards shown to drastically affect transportation networks is earthquakes. The criticality of proper functioning of the transportation network following earthquake events is so transportation for rescue workers, construction repair teams, and disaster relief efforts can be provided.

In order to predict the functionality of transportation networks following a seismic event, performance of embankments under real ground motions needs to be well understood. Understanding such performance can be realized using experimental testing or finite element analysis. Cost and limitations in laboratory capabilities hinder the possibility of conducting large experimental tests of embankments. Accurate numerical models, which are informed by observations of performance in previous earthquakes, can serve as suitable substitutes to experimental testing. This study investigates embankment performance under earthquake loading using numerical finite element models. Although extensive analytical modeling of pavements and embankments has been conducted for performance assessment under cyclic traffic loading, there is lack of analytical studies for evaluating embankment response under seismic loading. With improved understanding of embankment performance under earthquake loading, more informed planning efforts can be realized for post-disaster recovery. Traditionally, the effectiveness of a transportation network is primarily assessed by the level of bridge damage. Although bridge damage assessment is critical to understanding functionality of a transportation network, it is inaccurate to only rely on bridge damage data for such an assessment; this is because performance of roads, approaches, and embankments can impair the performance of a network.

Design of highway embankments is mainly driven by empirical investigations, mechanistic data, and field tests collected by the American Association of State Highway Officials (AASHO) and other similar institutions. These empirical investigations are used to define the correlation between applied loads on embankments and expected damage resulting from these loads. Mechanistic data are the collected data related to the embankment response under various loading conditions. These data are related to different stress components, strains, and displacements. With recent advances in computational techniques and efficiency, analytical models have been significantly relied upon to investigate the behavior of embankments subjected to various natural hazards. Different analytical modeling approaches can be found, including for instance, finite element analysis approach [2] and elastic layer theory approach [3].

This study aims to add to existing literature by conducting a seismic assessment of embankments using real ground motions. Specifically, in this study, the goal is to develop a simple non-linear finite element models that can capture the main characteristic of the real embankment behavior. ABAQUS finite element software is used to build the model geometry and define material properties. Once the model is developed, 44 earthquake ground motions from the FEMA P695 [4] database are then scaled based, assuming the embankment is located in Colorado. The records are then used to evaluate various performance levels.

1.2 Field Observations from Historical Events

The performance of highway embankments during earthquakes has received considerable attention. The damage is typically classified in relation to any type of failure introduced due to the vertical movement of the road with respect to its initial position. A common cause of such failure is vertical fault rupture (surface faulting). It is worth noting that in some earthquakes, fault rupture in an embankment never occurs simply because the embankment does not cross the fault. The damage that could occur due to vertical surface faulting could extend to include the pavement, subgrade, and base materials. While only minor cracks in the road typically occur because of surface faulting, since roads typically do not cross a fault line, large fault slip deformations could cause large differential movements and, subsequently, extensive failures. Examples of surface faulting failures—minor, moderate, and major—are shown below in Figure 1.1 and Figure 1.2 from the 1989 Loma Prieta and the 1999 Kocaeli earthquakes, respectively.

Figure 1.1 Surface faulting, Kocaeli [5] obtained from NISEE

Figure 1.2 Surface faulting, Kocaeli [5] obtained from NISEE

In addition to vertical differential movements, lateral movements can also occur. This failure is typically caused by shear failure developed due to shear loading. An example of a shear failure, classified as lateral movement/cracking damage, is shown in Figure 1.3, which was taken after the 2010 Chile earthquake. The centerline of the road is no longer aligned and shows large lateral offsets. Other types of failure exist, including longitudinal and transverse cracking, longitudinal or transverse ridges or overlaps, settlements, and others. An example of a tensile crack is shown in Figure 1.4. A detailed description of these types of failures with corresponding images describing the failure can be found in Lewis [7].

Figure 1.3 Shear failure, Chile (Lewis [7])

Figure 1.4 Tensile crack on the road surface due to the 2008 Wenchuan earthquake [6]

2. MODEL DESCRIPTION

Various simulation techniques exist for conducting numerical finite element simulation of embankments. These include the discrete element method (DEM) [6], as well as more specialized finite element software, such as PLAXIS 2D [8,9]. One of the common finite element packages used to analyze the highway embankments is ABAQUS finite element software. It offers the required tools to investigate the embankment components under the earthquake loads. Therefore, this software is utilized here to build a highway embankment and apply the earthquake loads.

2.1 Investigated Model

The investigated model is a two-lane highway on an embankment that consists of one middle section and two supporting shoulders. The middle section consists of two layers of hot-mixed asphalt (HMA), which are located at the top of the embankment. Beneath the HMA layers there is a base layer, which comprises of a granular layer, compacted subgrade layer and a natural layer. The shoulders are built to ensure the stability of the main embankment components, and the selected slope of these shoulders are 3:1 based on the IDOT manual [10]. Shoulders are built using the natural subgrade layer material. Figure 2.1 shows the components and depths of the investigated embankment. Values are chosen based on an average value of commonly used field materials and a silty-sand soil composition.

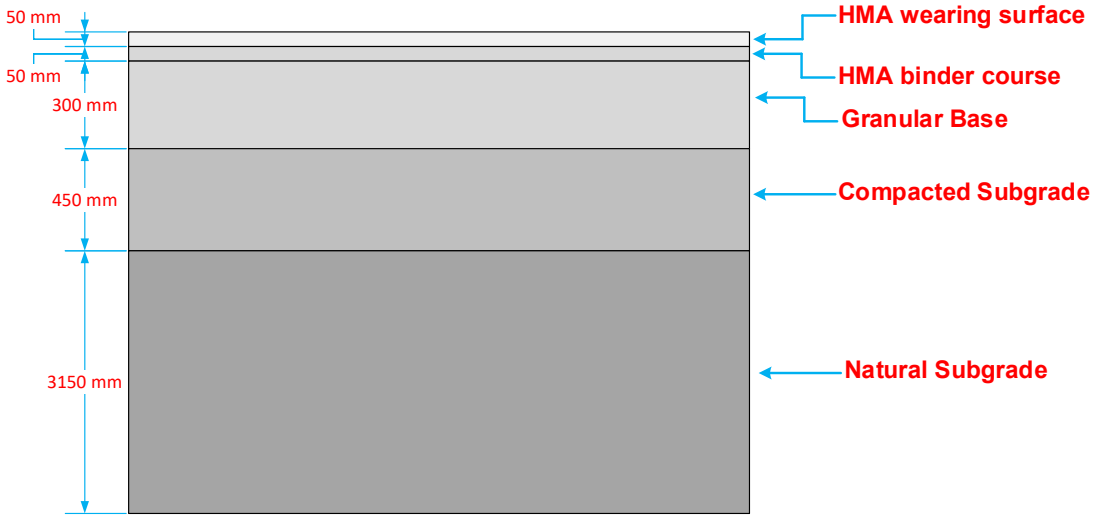

Figure 2.1 Various pavement layers

2.2 Material Model

Although embankment layers can experience inelastic deformations, the material properties for the granular base, compacted subgrade, and natural subgrade are assumed to be linear elastic for simplicity. This assumption can be valid if the stresses in these layers are below the inelasticity limit. Based on the resulting stresses in the investigated embankment, the shear stresses that cause the slip between the embankment layers are less than their value in the HMA layers. Therefore, the HMA layers were modeled using viscoelastic material. Table 2.1 shows the material properties for different layers of the investigated embankment based on Lewis' work [7].

Table 2.1 Material properties for different embankment layers

	Material Type	Elastic Modulas (MPa)	Poisson's ratio
HMA Wearing Surface	Viscoelastic	17,600	0.40
HMA Binder Course	Viscoelastic	14,400	0.40
Granular Base	Linear-elastic	300	0.35
Compacted Subgrade	Linear-elastic	100	0.35
Natural Subgrade	Linear-elastic	50	0.35

2.3 Model Non-Linearity

The non-linearity in the presented model includes both the material inelasticity and geometric non-linearity. The geometric non-linearity includes the P-delta effect throughout the analysis, which increases the resulted deformation in the model and amplifies the actions produced. Material inelasticity is considered throughout the viscoelastic model of the HMA layers.

In this analysis, a friction with slip model is used to capture the inelastic behavior of the HMA layers, which consist of a linear stage similar to the basic friction model and a specified shear stress limit in which slip will occur. The shear stress limit value is assumed to be 1.415 MPa, based on the study conducted by Romanoschi and Metcalf [11]. Figure 2.2 shows this study's implemented friction with slip model, which is used for the interface between the two HMA layers. This model is used to introduce the sliding behavior between the HMA layers when the shear stress reaches the slip limit. In addition, slipping and sticking in this model can be reversed based on the value of the current shear stress between the two surfaces.

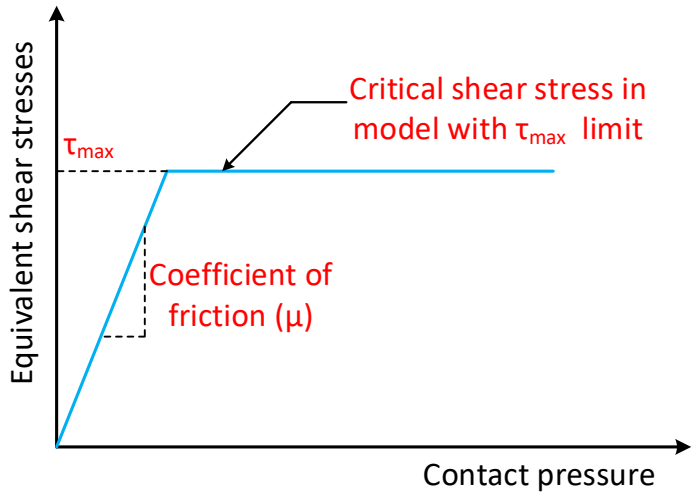

Figure 2.2 Coulomb friction with slip model

2.4 Presented Model Limitations

The presented model has limited applicability based on the type of the investigated problem. Using linear elastic material properties, the granular base, compacted subgrade, and natural subgrade layers are only valid if the earthquake demand is limited, which is the case for the investigated region (Colorado). The two-dimensionality of the presented model is considered as another simplification, which ignores longitudinal effects of the embankment on the resulting stresses and displacements.

3. GROUND MOTION SELECTION

To assess seismic performance of the highway embankment, a set of ground motions are selected and applied to the finite element model that has been developed based on the discussion in previous sections. The ground motions are applied to the embankment at the natural grade lower level, as shown in Figure 3.1, in the form of acceleration in x direction.

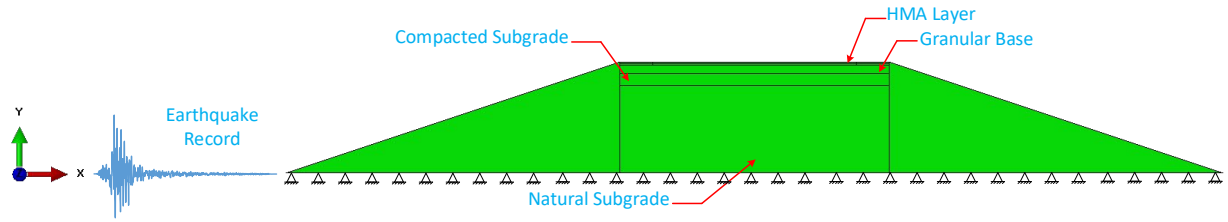

Figure 3.1 Ground motion application on embankment

3.1 Ground Motion Selection

FEMA P695 [4] far field ground motions are selected to investigate the seismic performance of the embankment. This set of ground motions comprises 44 earthquake records (two horizontal motions sets, each with 22 ground motions). All the selected ground motions are far field records with distances greater than 10 km. Along with the record ID number, Table 3.1 shows a summary of selected ground motions, which will be used in the following sections: magnitude, year, name, and fault type of each earthquake, as well as their recording stations and epicentral distance. Magnitudes of selected earthquakes range from M6.5 to M7.6, with an average magnitude of M7.0. The site classes of these earthquakes are either D and C, based on NEHRP classification. These earthquakes are selected to have a peak-ground acceleration range from 0.21g to 0.82g.

As mentioned, for each ground motion, there are two horizontal components and one vertical component. In this report, both horizontal components are utilized: notation “X” used for the first component and notation “Y” used for the second component. Pacific Earthquake Engineering Research (PEER) Center strong motion database is used to obtain all 44 ground motion records. A 5% damping ratio is used to scale the selected ground motions.

Table 3.1 Far field ground motions based on FEMA P695 [4]

ID No.	Earthquake				Recording station	Epicentral distance (Km)
	Magnitude	Year	Name	Fault Type		
1	6.7	1994	Northridge	Thrust	Beverly Hills - Mulhol	13.3
2	6.7	1994	Northridge	Thrust	Canyon Country-WLC	26.5
3	7.1	1999	Duzce, Turkey	Strike-slip	Bolu	41.3
4	7.1	1999	Hector Mine	Strike-slip	Hector	26.5
5	6.5	1979	Imperial Valley	Strike-slip	Delta	33.7
6	6.5	1979	Imperial Valley	Strike-slip	El Centro Array #11	29.4
7	6.9	1995	Kobe, Japan	Strike-slip	Nishi-Akashi	8.7
8	6.9	1995	Kobe, Japan	Strike-slip	Shin-Osaka	46
9	7.5	1999	Kocaeli, Turkey	Strike-slip	Duzce	98.2
10	7.5	1999	Kocaeli, Turkey	Strike-slip	Arcelik	53.7
11	7.3	1992	Landers	Strike-slip	Yermo Fire Station	86
12	7.3	1992	Landers	Strike-slip	Coolwater	82.1
13	6.9	1989	Loma Prieta	Strike-slip	Capitola	9.8
14	6.9	1989	Loma Prieta	Strike-slip	Gilroy Array #3	31.4
15	7.4	1990	Manjil, Iran	Strike-slip	Abbar	40.4
16	6.5	1987	Superstition Hills	Strike-slip	El Centro Imp. Co.	35.8
17	6.5	1987	Superstition Hills	Strike-slip	Poe Road (temp)	11.2
18	7.0	1992	Cape Mendocino	Thrust	Rio Dell Overpass	22.7
19	7.6	1999	Chi-Chi, Taiwan	Thrust	CHY101	32
20	7.6	1999	Chi-Chi, Taiwan	Thrust	TCU045	77.5
21	6.6	1971	San Fernando	Thrust	LA - Hollywood Stor	39.5
22	6.5	1976	Friuli, Italy	Thrust	Tolmezzo	20.2

3.2 Record Scaling

The selected records are scaled based on the structure's fundamental period in accordance with AASHTO [12] and NHI [13]. To scale the earthquake motions, the mean of the ground motion response spectra is developed and matched to the design response spectrum for the embankment location. The selected location of the embankment is Denver, Colorado. The soil type for this area is selected as stiff. The USGS database and AASHTO [12] Guide Specifications are used to develop the design response spectrum. Figure 3.2 shows the response spectrum for all far field ground motion records before and after the scaling.

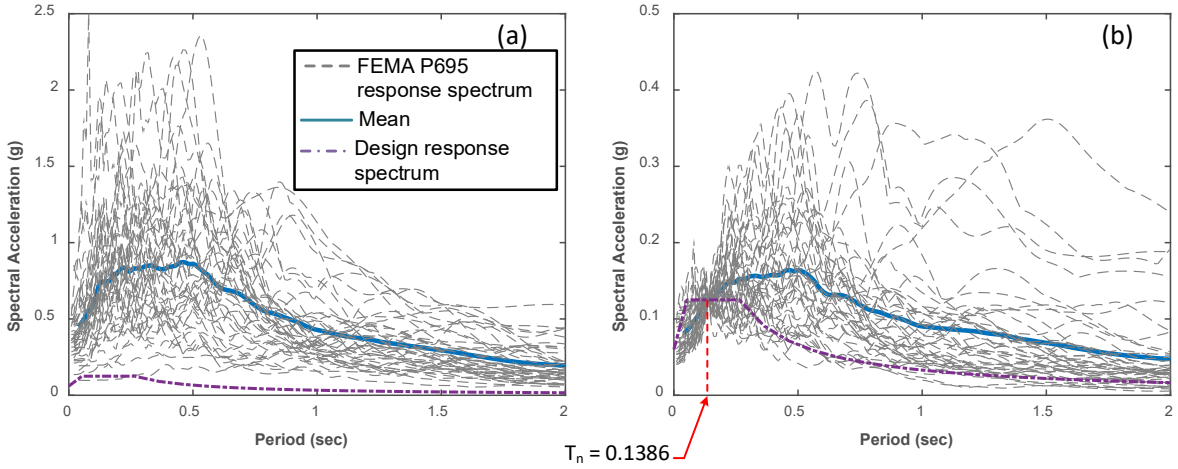

Figure 3.2 FEMA P695 far field records' response spectrum vs. AASHTO design response spectrum: a) before scaling and b) after scaling

3.3 Failure Limit State Definitions

Assessment of embankment performance under an earthquake hazard is essential for understanding the transportation network resilience. Defining failure limit states is a key factor in the assessment process. These limit states are compared with the analytical model results to classify the failure type of the investigated embankment. Commonly, two main components are considered to evaluate earthquake damage: a) maximum observed displacement, which usually occurs during the earthquake, and b) residual displacement, which is measured after earthquake occurrence.

Two different sets of limit states for highway embankments can be used to define their performance during earthquakes. The first set is based on the local pavement components' performance, and includes functional damage without any structural damage, structural damage that requires rehabilitation, and structural damage that requires replacement. This set considers both the horizontal and lateral displacements of the embankment, as well as settlement deformations. It also utilizes other different failure components to define these three limit states, as shown in Table 3.2. Only vertical and lateral displacement failures are considered in this study due to the presented model limitations. The second set of limit states is based on the global performance of the investigated embankment, and includes only slight, moderate, extensive, and complete damage limit states. This set considers only the permanent displacement of the investigated embankment, as shown in Table 3.3.

Table 3.2 Limit states based on local pavement components' performance (mm) [7]

	Functional damage without any structural damage	Structural damage that requires rehabilitation	Structural damage that requires replacement
Lateral displacement	6	22	22
Vertical displacement	6	27	27
Longitudinal cracks	8	27	27
Transverse cracks	9	25	25
Longitudinal ridge	9	28	28
Transverse ridge	9	30	30
Longitudinal overlap	13	32	32
Transverse overlap	13	32	32
Settlement - no cracking	9	28	28
Settlement – cracking	10	24	24
Settlement holes	18	33	33

Table 3.3 Limit states based on global performance (mm) [14]

	Slight	Moderate	Extensive	Complete
Permanent deformation	25	76	152	305

4. RESULTS AND DISCUSSIONS

This section summarizes results from a finite element model of embankments under seismic load. It highlights the seismic performance of embankments, including various observed failures in different embankment layers. Residual deformations were measured for each ground motion record. A comparison between embankments response and various damage limit states is used to characterize embankment damage.

4.1 State of Stress

In this section, stresses at natural subgrade, compacted subgrade, granular base, and HMA layers are discussed in detail for the 4-meter embankment under the 44 FEMA P-695 far field records. Figure 4.1 shows the von Misses stresses in MPa for the investigated embankment under the "Y" component of the Superstition Hills earthquake record. Stress concentrations at right- and left-hand side of the HMA binder course, granular base, and compacted subgrade layers can be noticed. The maximum von Misses stress is recorded at the HMA binder course layer with a value of 0.0426 MPa. As expected, the von Misses stresses decrease in the middle of the embankment layers and at the lower edge of the natural subgrade layer.

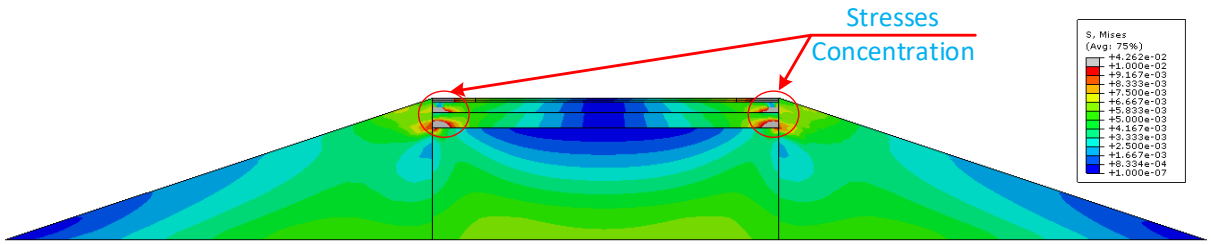

Figure 4.1 von Misses stresses of the embankment under Superstition Hills, Poe Road station earthquake record, "Y" component

Figure 4.2 shows the shear stresses on different investigated embankment layers in MPa for the previously mentioned earthquake record. Unlike the von Misses stresses, the shear stresses concentrate at the middle of the embankment layers. The value of the shear stresses decreases at the natural subgrade layer. Even though the maximum value of the shear stress is found at the interface between the HMA wearing surface and binder course layers, the value of this stress is less than the slip limit specified by Romanoschi and Metcalf [11], which equals to 1.415 MPa. Therefore, no slip between the two HMA layers is expected in this case. Moreover, the maximum shear stress resulting from applying all the FEMA P695 records on the investigated embankment is also less than the previously mentioned slip limit.

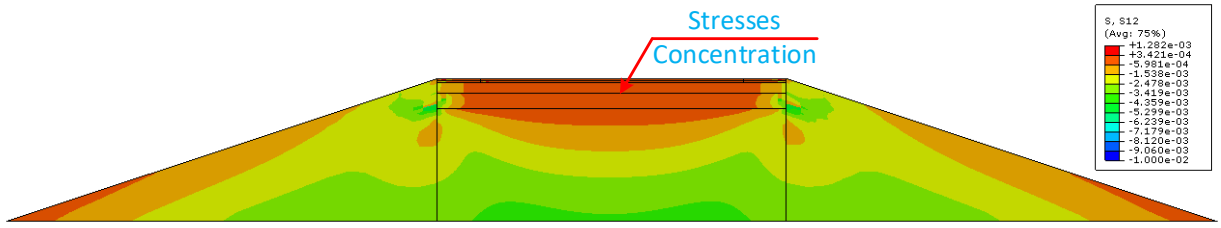

Figure 4.2 Shear stresses of the embankment under Superstition Hills, Poe Road station earthquake record, "Y" component

4.2 Failure Assessment

As mentioned, the two main embankment displacements that will be measured to assess the seismic performance are the maximum and residual displacements. Displacement at the top surface of the embankment is used to represent both the peak and residual displacement. Figure 4.3 shows the lateral displacement distribution of the investigated embankment under the Superstition Hills earthquake record for the "Y" component. It can be noted that displacement magnitude at the top layers is significantly higher than the natural subgrade lower level, as shown in the figure. The lateral displacement response for the rest of the 44 ground motions are listed in Appendix A.

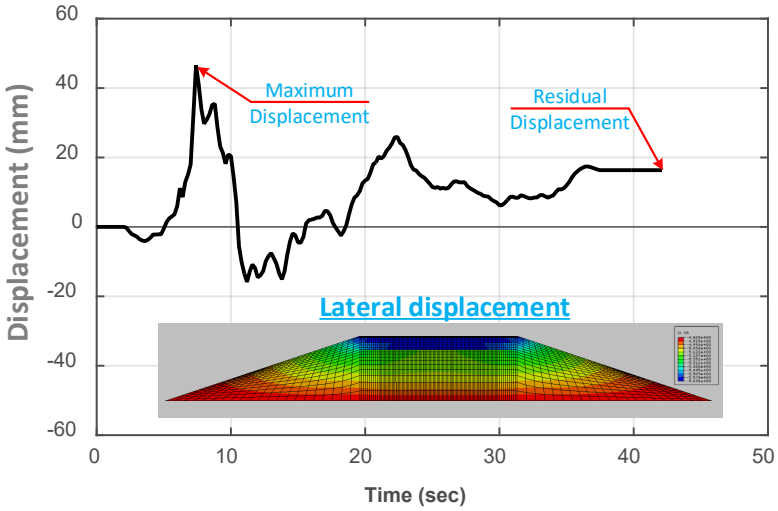

Figure 4.3 Lateral displacement of the embankment under Superstition Hills, Poe Road station earthquake record, "Y" component

Figure 4.4 shows the vertical displacement distribution for the investigated embankment under the Superstition Hills earthquake record for the "Y" component. Unlike the lateral displacement distribution, the magnitude of the vertical displacement is only higher at the edges of the top layers and in opposite directions. It can also be noted that displacement magnitude is minimal compared with the lateral displacement. Therefore, the damage in the embankment is mostly related to the lateral displacement.

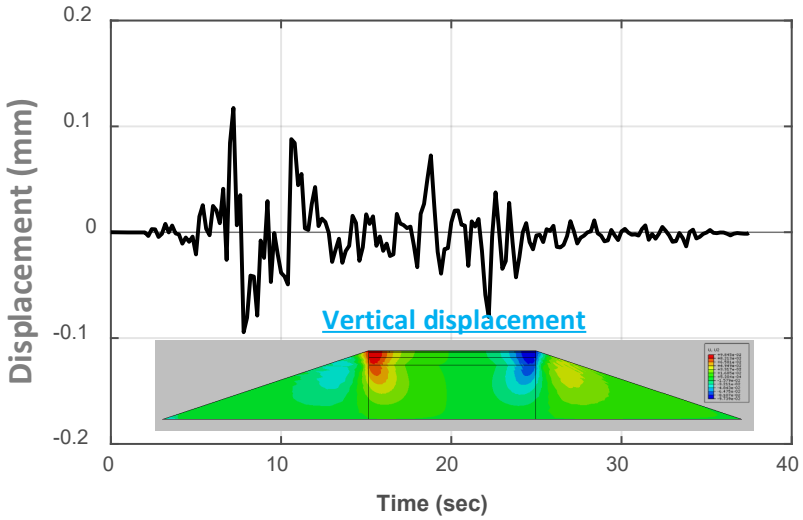

Figure 4.4 Vertical displacement of the embankment under Superstition Hills, Poe Road station earthquake record, "Y" component

4.2.1 Performance of Local Pavement Components

The first set of limit states is based on local pavement components performance. Due to the limitation of the presented model, only lateral and vertical displacements are considered as a performance indicator. Figure 4.5 displays the maximum lateral displacements of the investigated embankment under the 44 FEMA P695 ground motions. The lowest recorded value is for the Loma Prieta earthquake at the Capitola recording station in the "Y" direction and equals 3.32 mm, which corresponds to no functional damage. The highest recorded value is for the Kocaeli, Turkey, earthquake at Arcelik recording station in "Y" direction and equals 912.66 mm, which corresponds to total structural damage. As noted in Figure 4.5, in most of the earthquake scenarios, the maximum lateral displacements are higher than the structural damage limit state, which requires a replacement of the embankment. In other words, the case of no functional damage occurs in four earthquake scenarios, the functional damage without structural damage takes place at 23 earthquake scenarios, and the functional damage with structural damage takes place at 17 earthquake scenarios.

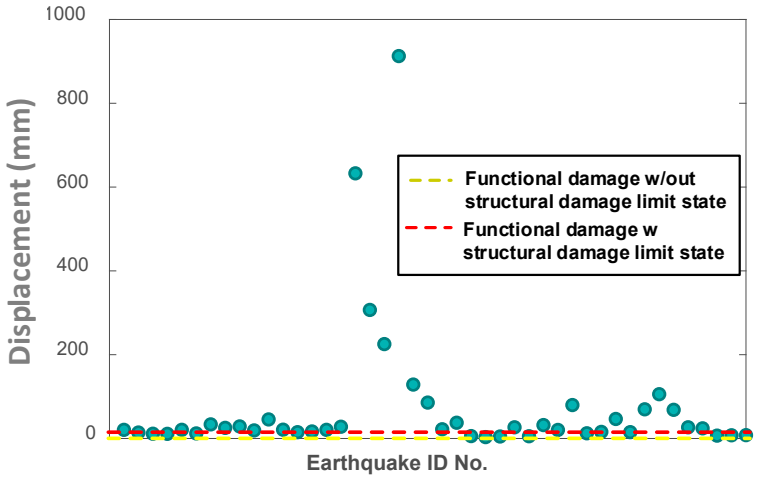

Figure 4.5 Lateral displacement of the embankment under FEMA P695 records

Figure 4.6 shows the maximum vertical displacements of the investigated embankment under the 44 FEMA P695 ground motions. The lowest recorded value is for the Loma Prieta earthquake at the Capitola recording station in the "Y" direction and equals 0.08 mm, which refers to no functional damage. The highest recorded value is for the Kocaeli, Turkey, earthquake at the Arcelik recording station in the "Y" direction and equals 0.18 mm, which also refers to no functional damage. As noted in Figure 4.6, all the earthquake scenarios will not generate any damage to the embankment. This is because the applied ground motions are in the "X" direction, as mentioned, and no accelerations are applied in the vertical direction.

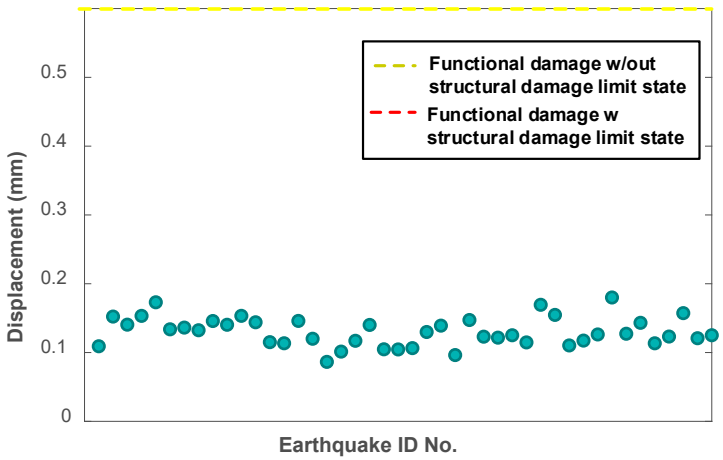

Figure 4.6 Vertical displacement of the embankment under FEMA P695 records

4.2.2 Performance of Global Embankment

The second set of limit states is based on global performance of the investigated embankment. Figure 4.7 shows the lateral residual displacements of the investigated embankment under the 44 FEMA P695 ground motions. The lowest recorded value is for the Chi-Chi, Taiwan, earthquake at the TCU045 recording station in the "Y" direction and equals 0.15 mm, which corresponds to no damage. The highest recorded value is for the Kocaeli, Turkey, earthquake at the Arcelik recording station in the "Y" direction and equals 82.28 mm, which is considered as moderate damage. As noted in Figure 4.7, all the earthquake scenarios will not generate any extensive or complete damage to the embankment.

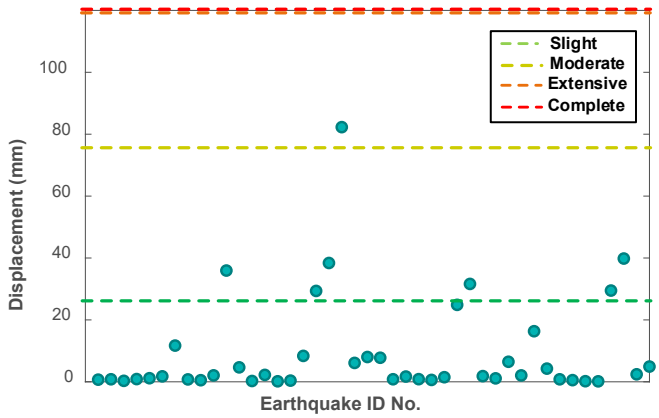

Figure 4.7 Residual lateral displacement magnitude of the embankment under FEMA P695 records

5. CONCLUSION AND DISCUSSIONS

The response of a 4-meter high embankment under different earthquake scenarios has been investigated. Two different damage limit states were utilized: one is based on performance of local pavement components; the other is based on global performance of the investigated embankment. Finite element models were used to study the seismic response of the embankment. State of stresses and failure assessment were presented. Several findings were made and are summarized below:

- The maximum von Misses stress recorded for most of the earthquake records were at the HMA binder course layer.
- The maximum shear stress resulting from applying all the FEMA P695 records on the investigated embankment was less than the shear slip limit.
- Magnitude of the lateral displacement was significantly higher at the top layers than the natural subgrade lower level.
- Magnitude of the vertical displacement was only higher at the edges of the top layers.
- Assessment of local pavement components showed that the investigated embankment suffered functional damage associated with structural damage from 17 earthquake scenarios.
- Assessment of global performance showed that the investigated embankment only experienced slight and moderate damage.

REFERENCES

[1] C. M. Duke, "An Earthquake Hazard Plan for Lifelines," in: *Lifeline Earthq. Eng. Curr. State Knowl*., ASCE, New York, NY, 1981.

[2] S. Helwany, J. Dyer, and J. Leidy, "Finite-Element Analyses of Flexible Pavements," *J. Transp. Eng.* 3 (1998) 491–499.

[3] I.L. Al-qadi, and H. Wang, *Evaluation of Pavement Damage due to New Tire Designs*, 2009.

[4] FEMA P695, *Quantification of Building Seismic Performance Factors*, 2009.

[5] National Information Service for Earthquake Engineering (NISEE), The Earthquake Engineering Online Archive, (n.d.). http://nisee.berkeley.edu/elibrary/.

[6] J. Wang, Q. Li, C. Yang, and C. Zhou, "Dynamic response and damage character of road embankment under strong earthquake," *Int. J. Distrib. Sens. Networks*. 14 (2018). doi:10.1177/1550147718794611.

[7] A.L. Lewis, *Embankment Performance Under Earthquake Loading*, University of Illinois at Urbana-Champaign, 2011.

[8] B.H. Maula, and L. Zhang, "Assessment of Embankment Factor Safety Using Two Commercially Available Programs in Slope Stability Analysis," *Procedia Eng*. 14 (2011) 559–566. doi:10.1016/j.proeng.2011.07.070.

[9] Y. Zhu, K. Lee, and G.H. Collison, "A 2D Seismic Stability and Deformation Analysis, in: Geo-Frontiers Congr. 2005, *Earthq. Eng. Soil Dyn*., Austin, Texas, United States, 2005: pp. 1–15.

[10] IDOT Design Manual, Chapter 38: Roadside Safety, 2002.

[11] S. Romanoschi, and J. Metcalf, "Effects of Interface Condition and Horizontal Wheel Loads on the Life of Flexible Pavement Structures," *Transp. Res. Board Natl. Acad*. 1778 (2001) 123–131. https://doi.org/10.3141/1778-15.

[12] American Association of State Highway and Transportation Officials, *AASHTO LRFD Bridge Design Specifications*, Washington, DC 20001, 2012.

[13] E. Kavazanjian, J.-N.J. Wang, G.R. Martin, A. Shamsabadi, I. (Po) Lam, S.E. Dickenson, and C.J. Hung, *LRFD Seismic Analysis and Design of Transportation Geotechnical Features and Structural Foundations Reference Manual*, FHWA-NHI-11-032, Washington, D.C. 20590, 2011.

[14] S.D. Werner, C.E. Taylor, S. Cho, J. Lavoie, C. Huyck, C. Eitzel, H. Chung, and R.T. Eguchi, *REDARS 2: Methodology and Software for Seismic Risk Analysis of Highway Systems*, 2006.

APPENDIX

This section shows the embankment responses under all the 22 ground motions, which are selected based on FEMA P-695 far field records for both horizontal directions (X and Y). Displacement response was used to assess the response of the embankment, which had been used to evaluate the peak displacement and the residual displacement for the embankment.

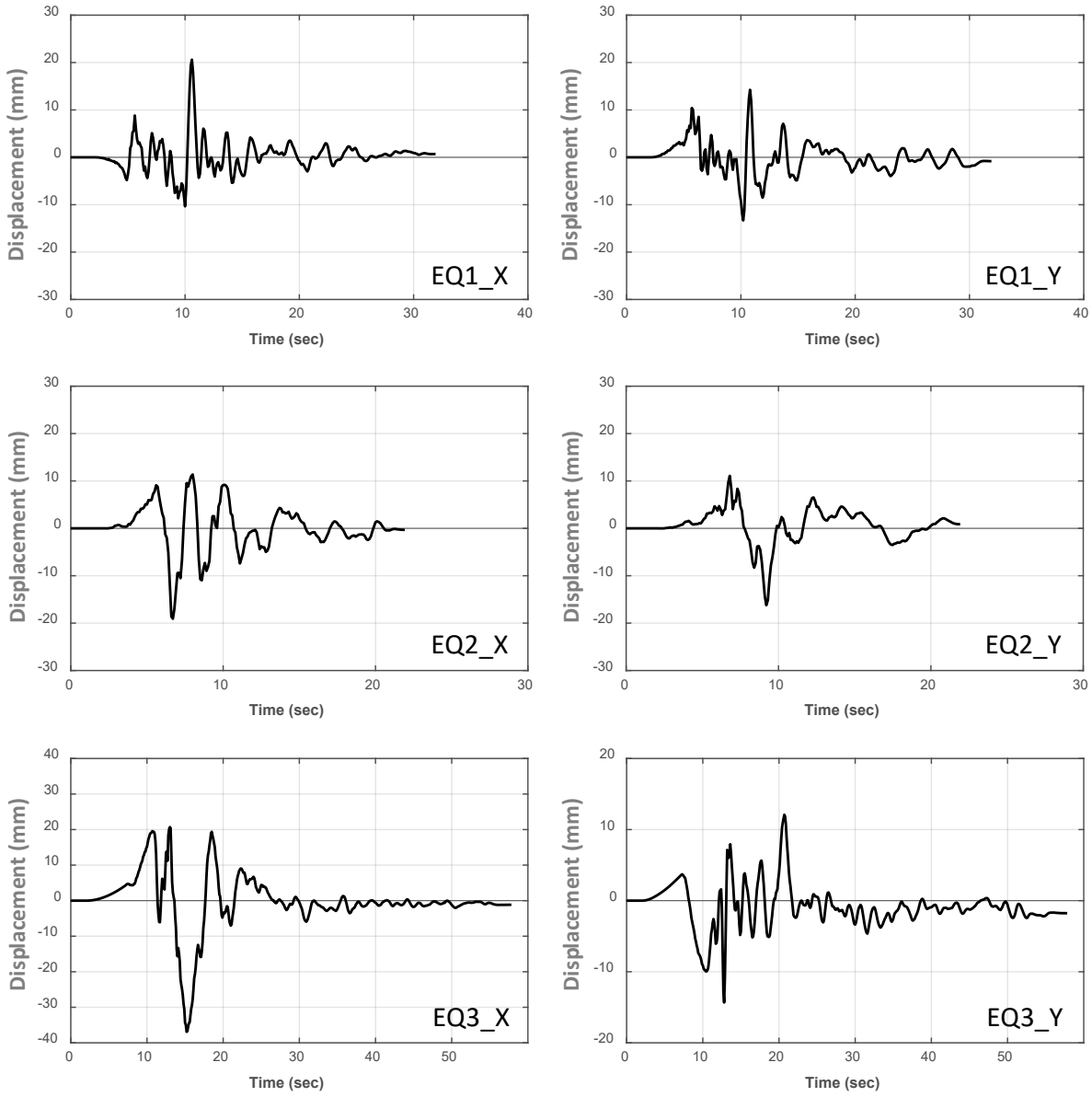

Figure A.1 Embankment response under earthquake ID from 1 to 3

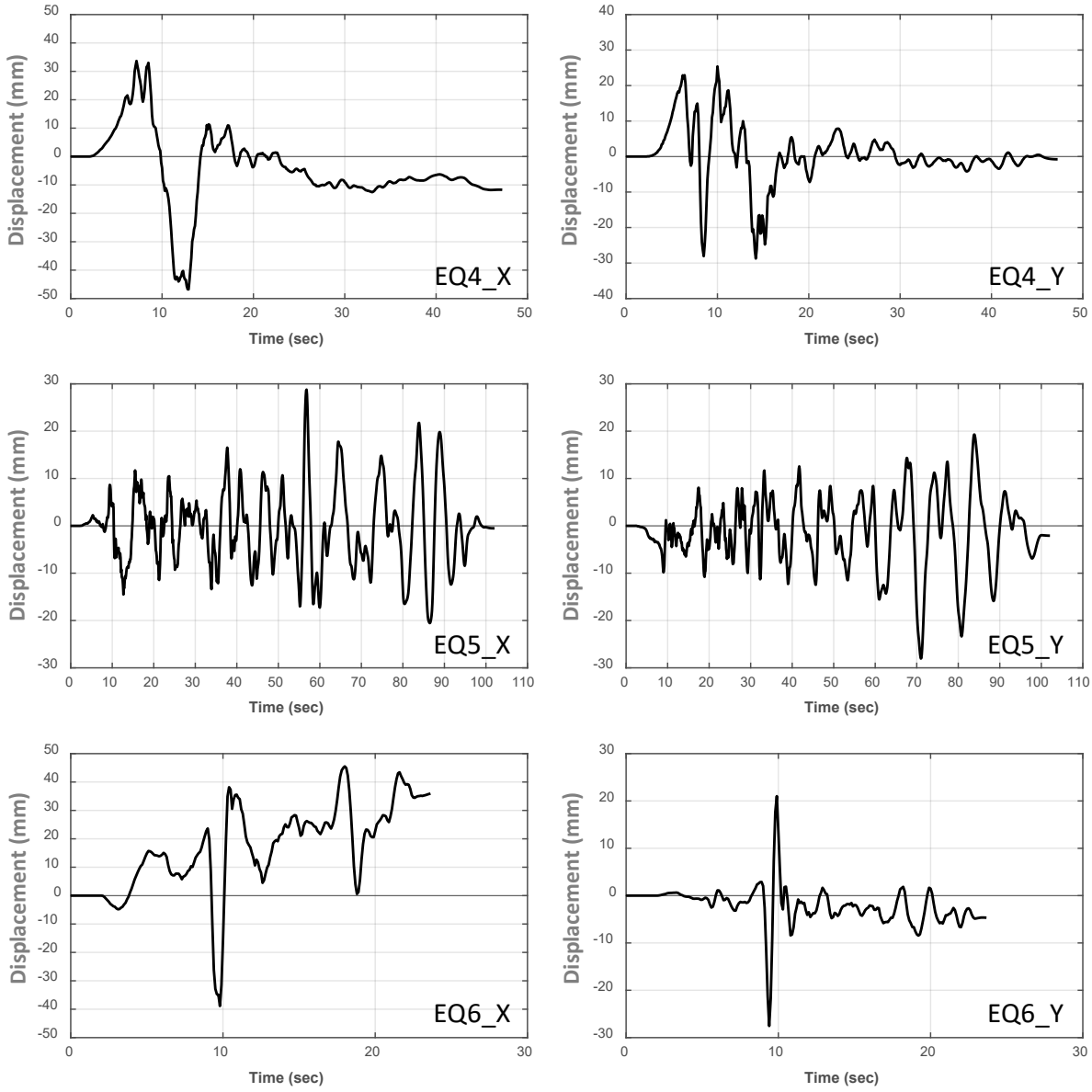

Figure A.2 Embankment response under earthquake ID from 4 to 6

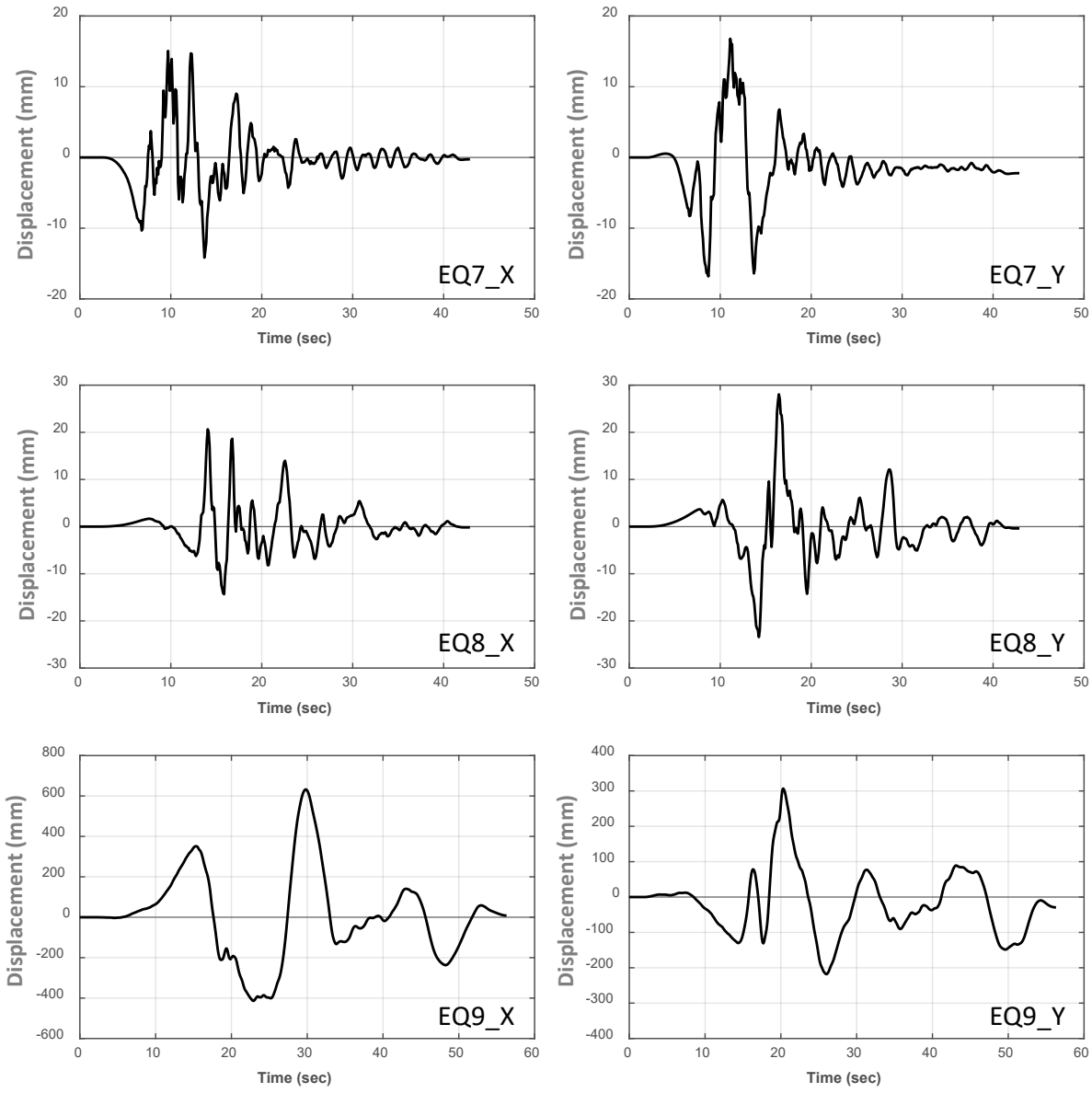

Figure A.3 Embankment response under earthquake ID from 7 to 9

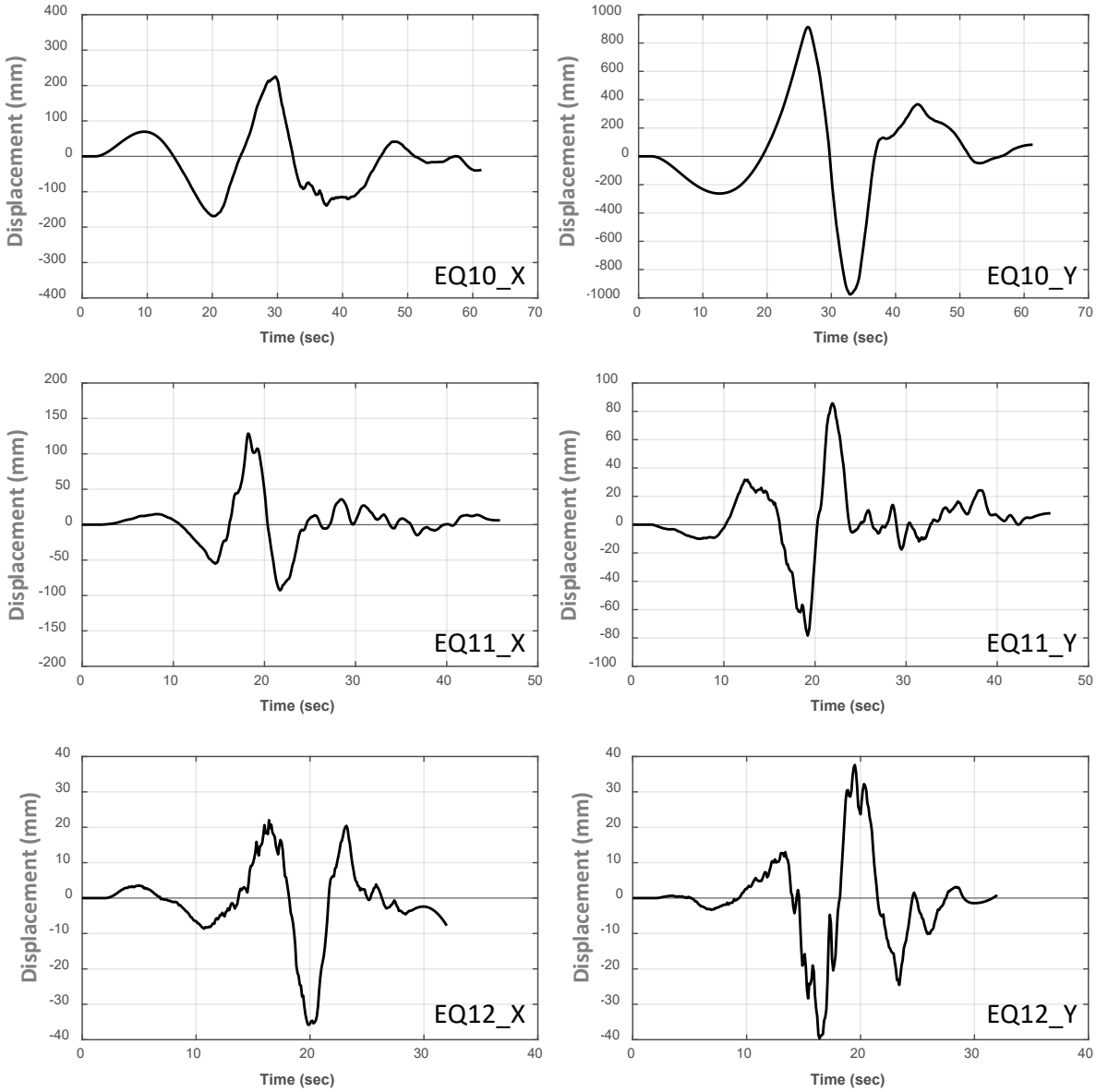

Figure A.4 Embankment response under earthquake ID from 10 to 12

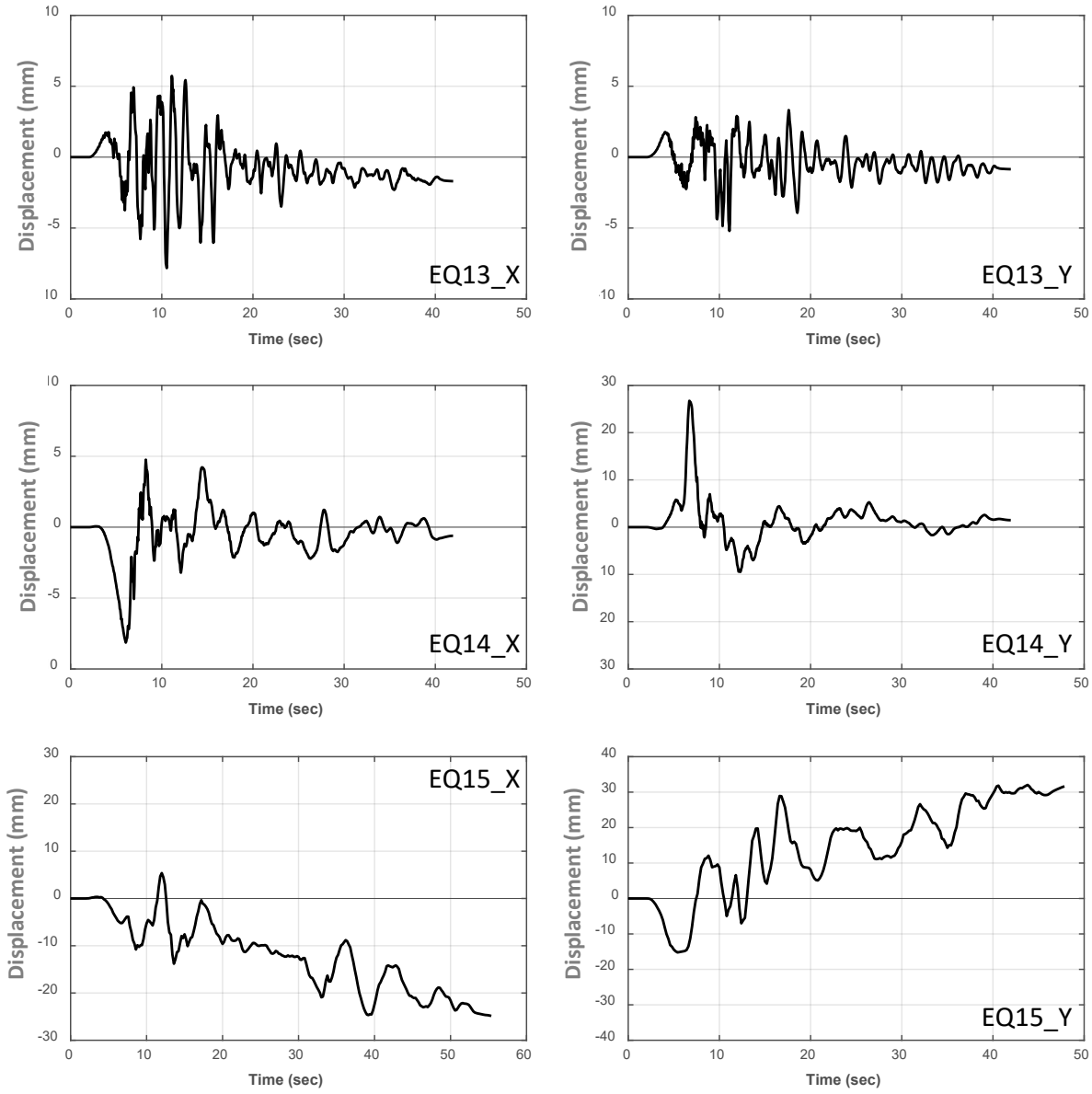

Figure A.5 Embankment response under earthquake ID from 13 to 15

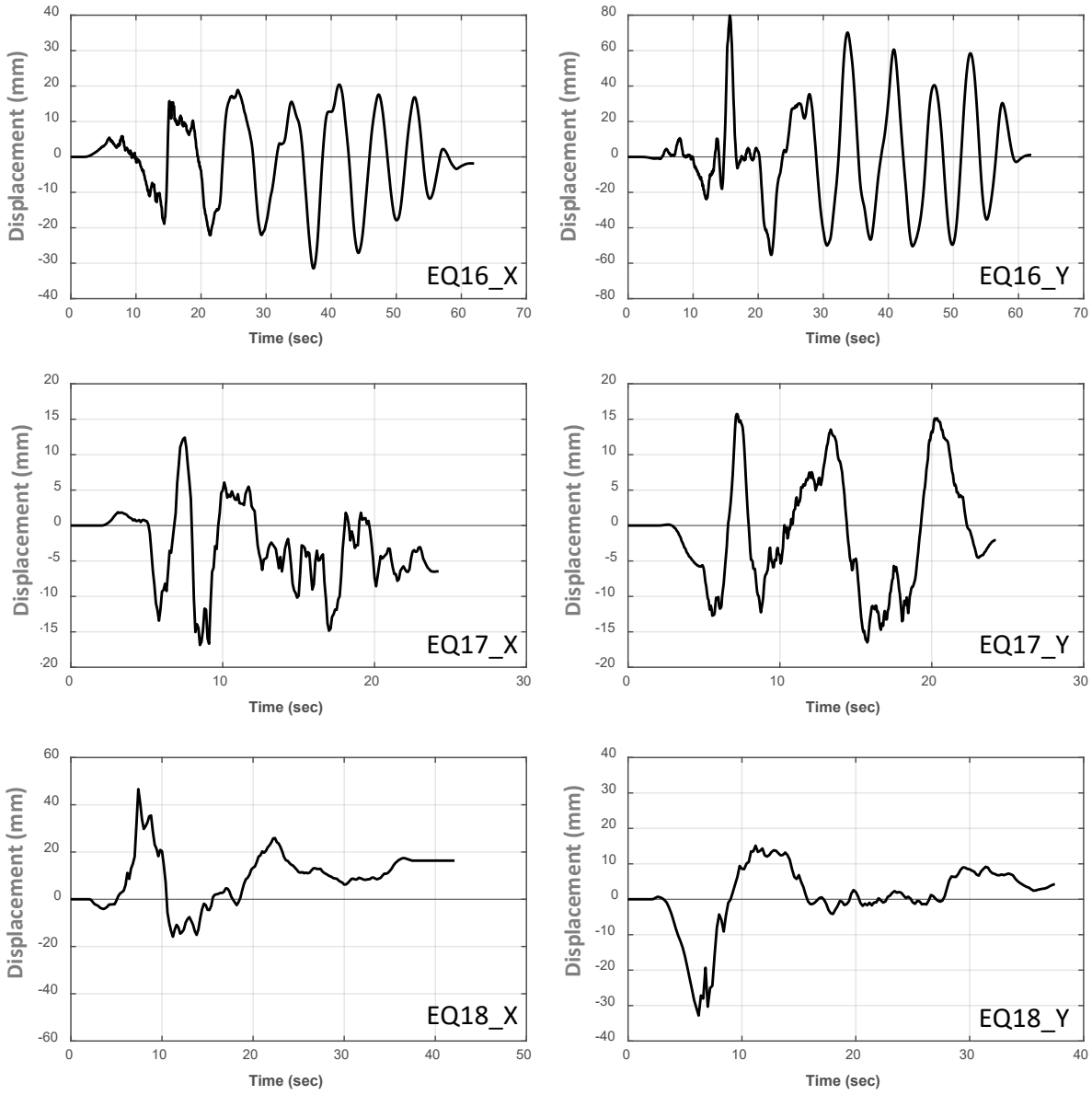

Figure A.6 Embankment response under earthquake ID from 16 to 18

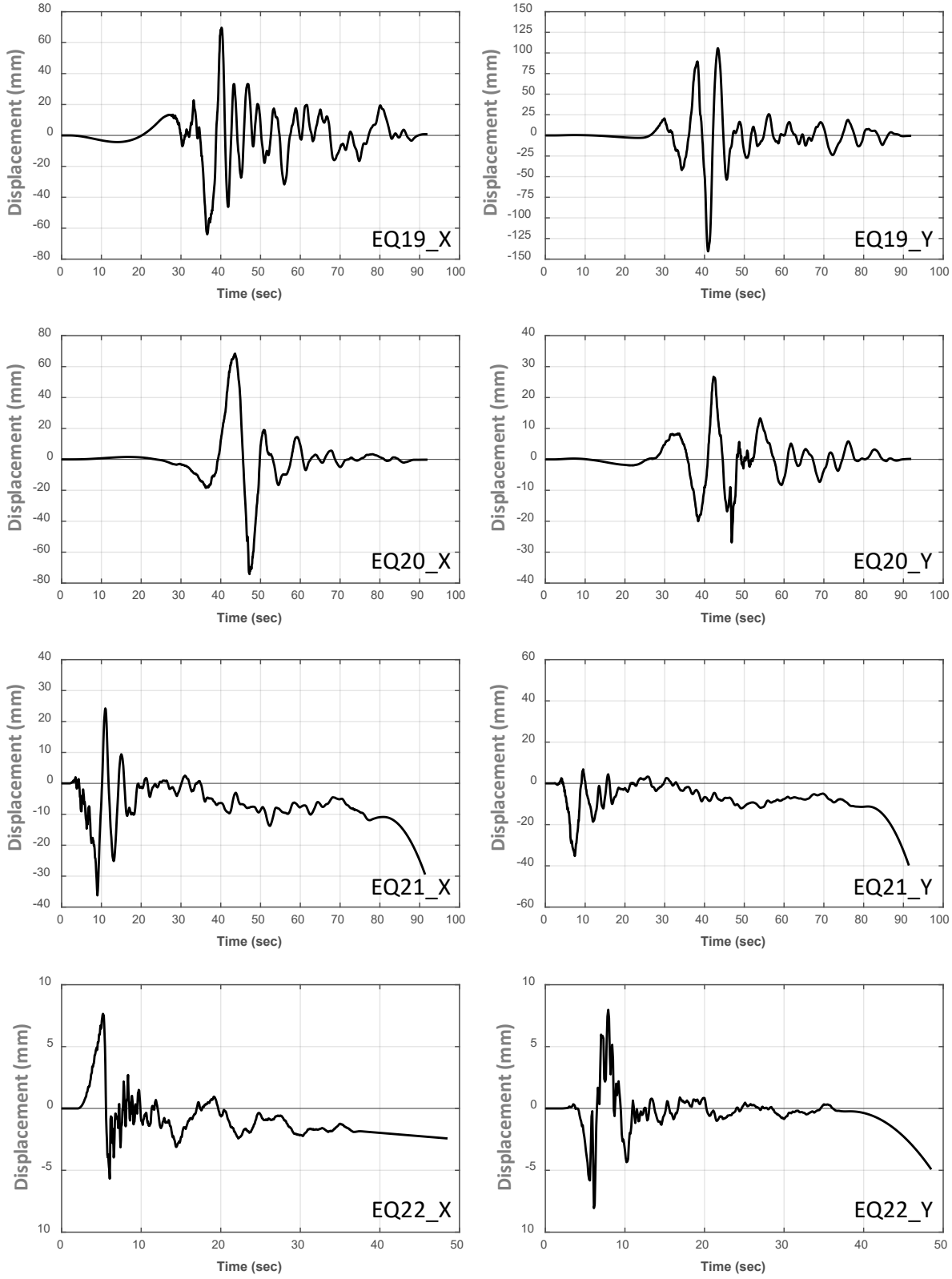

Figure A.7 Embankment response under earthquake ID from 19 to 22